Production of Fock Mixtures in Trapped Ions for Motional Metrology

Antonis Delakouras[1], Daniel Rodríguez[2,3] and Javier Cerrillo[4]‡

[1]Humboldt Universität zu Berlin, Berlin, Germany

[2]Departamento de Física Atómica, Molecular y Nuclear, Universidad de Granada, 18071, Granada, Spain

[3]Centro de Investigación en Tecnologías de la Información y las Comunicaciones, Universidad de Granada, 18071 Granada, Spain

[4]Área de Física Aplicada, Universidad Politécnica de Cartagena, Cartagena 30202 Spain

Abstract. We present a protocol to produce a class of non-thermal Fock state mixtures in trapped ions. This class of states features a clear metrological advantage with respect to the ground state, thus overcoming the standard quantum limit without the need for full sideband cooling and Fock-state preparation on a narrow electronic transition. The protocol consists in the cyclic repetition of red-sideband, measurement and preparation laser pulses. By means of the Kraus map representation of the protocol, it is possible to relate the length of the red sideband pulses to the specific class of states that can be generated. With the help of numerical simulations, we analyze the parametric regime where these states can be reliably reproduced.

1. Introduction

Trapped ions are a platform of reference for the implementation and testing of quantum information protocols [1,2], with several recent achievements in the quantum computing race [3]. Beyond quantum computation, quantum logic spectroscopy [4] has opened up a useful avenue in quantum metrology [5], both in the context of optical clocks [6] and force sensing [7–9]. Nevertheless, non-vanishing fluctuations of the motional ground state set a fundamental limit (standard quantum limit, SQL) in the precision of many quantum sensors.

An ongoing effort to improve the sensing capabilities of trapped ions is underway, with promising strategies arising in recent times. One of these consists in the use of non-thermal motional states. Squeezed states were one of the first workarounds to SQL that were proposed and implemented to great success [10] in the photonic context, and has been proposed [11, 12] and implemented [13–15] in the context of trapped ions. In order to avoid the accurate control of the phase of squeezed states with respect to the measured force, excited Fock states ($n = 1, 2, ...$) have recently
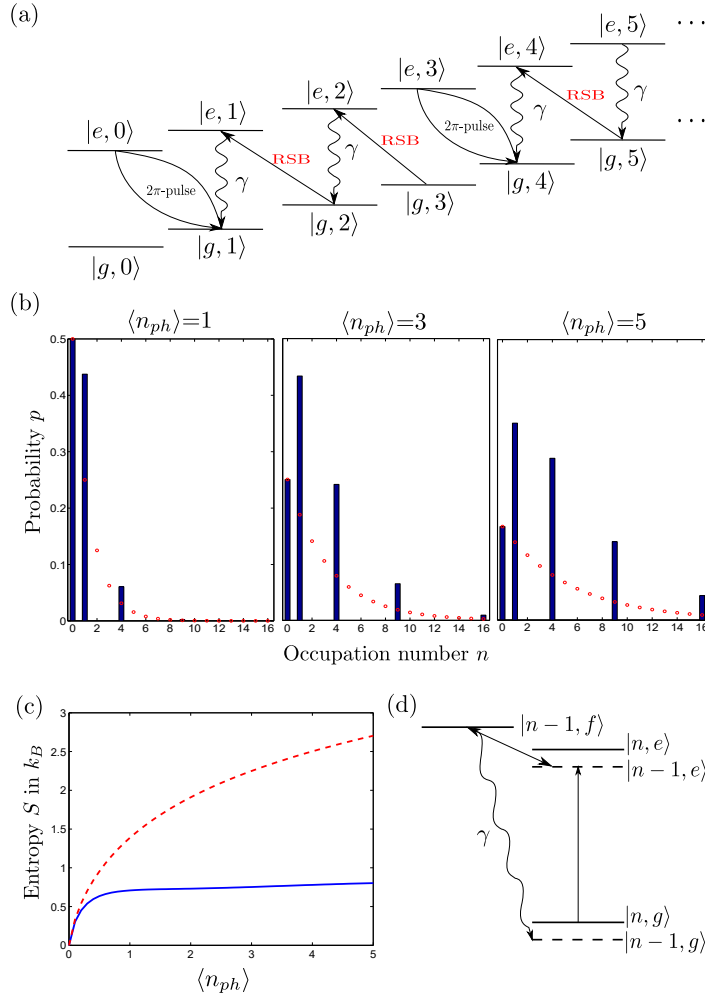
‡ Corresponding author: javier.cerrillo@upct.es

Figure 1. (a) Production process and energy levels of a trapped state for $n_0 = 1$. (b) Trapped (blue bars) and thermal (red dots) probability distributions for various values of $\langle n_{ph} \rangle$ and $n_0 = 1$ (associated with the trap series $0, 1, 4, 9, 16, \ldots$). (c) Thermal and trapped state entropy for $n_0 = 1$ as a function of $\langle n_{ph} \rangle$. (d) Experimental realisation through a third energy level with a fast decay rate back to the electronic ground state.

been proposed [16] as a means to achieve metrological advantages with respect to the ground state. Their production involves ground state cooling [17], often via a transition that resolves motional Fock states and therefore severely delays the cooling process. Although higher cooling rates can be obtained by applying electromagnetically induced transparency [18], they cannot be arbitrarily increased [19, 20] unless more elaborate implementations are considered [21].

Here we analyze a novel and simple protocol for the production of Fock state mixtures that circumvents the need for ground-state laser cooling and repeated blue-sideband cycles to prepare a specific Fock state. These mixtures, that we term *trapped states*, retain a significant metrological advantage with respect to the ground state. They feature a reduced entropy with respect to the states they were created from and,

in addition, their parity can be well defined. In this paper we explore in detail the production process as well as the properties of trapped states, which can be generated with red-sideband excitations although also blue-sideband excitations can be used.

The paper is structured as follows. In sec. 2 we present the protocol formally, we define the concept of trapped states, and also analyze their form in the special case of an initially thermal ion. Sec. 3 introduces the Kraus map representation of the protocol. In sec. 4 we explore the applicability of the trapped state in the context of quantum metrology and displacement sensitivity. In sec. 5 we extend the idea to the use of blue-sideband excitations. Finally, in sec. 6 we simulate the results numerically under realistic conditions by employing a Lindblad master equation and provide the final conclusions of the work.

2. Implementation of the Protocol

We consider implementation of our protocol in a trapped-ion architecture. Let us model the electronic degrees of freedom of a trapped ion with a two-level system: an electronic ground state $|g\rangle$ and an excited state $|e\rangle$, with transition frequency ω. Its motional degrees of freedom are approximated by a quantum harmonic oscillator of natural frequency ν. Control is exerted by means of a laser field of frequency ω_l that induces Rabi oscillations of frequency Ω and is characterized by a Lamb-Dicke parameter η [22]. The Hamiltonian in the rotating wave approximation (RWA) with respect to $\omega_l \sigma_z/2$ and taking $\hbar = 1$ is

$$H = \frac{\Delta}{2}\sigma_z + \nu a^\dagger a + \frac{\Omega}{2}\left[\sigma^+ D\left(i\eta\right) + \sigma^- D^\dagger\left(i\eta\right)\right], \tag{1}$$

where $\Delta = \omega - \omega_l$ is the detuning of the laser with respect to the transition, a is the annihilation operator of the harmonic oscillator, $D\left(\alpha\right) = \exp\left(\alpha a + \alpha^* a^\dagger\right)$ is the displacement operator, $\sigma^+ = |e\rangle\langle g|$, $\sigma^- = (\sigma^+)^\dagger$ are the spin raising and lowering operators respectively and $\sigma_z = 1 - 2\sigma^-\sigma^+$. The Lamb-Dicke regime is quantitatively expressed by $\eta\sqrt{\langle n_{ph}\rangle} \ll 1$, where $\langle n_{ph}\rangle$ is the average phonon number. In this regime, transitions that modify the motional state by more than a single phonon are strongly suppressed. In this limit, setting the detuning $\Delta = \nu$, and additionally performing a RWA with respect to $\nu\left(a^\dagger a + \sigma_z/2\right)$, yields the red sideband (RSB) Hamiltonian

$$H_{RSB} = \frac{i\eta\Omega}{2}\left(a\sigma^+ - a^\dagger\sigma^-\right), \tag{2}$$

also known as the the Jaynes-Cummings Hamiltonian [23]. It generates Rabi oscillations between states $|g,n\rangle \leftrightarrow |e,n-1\rangle$ at a frequency $\eta\Omega\sqrt{n}$.

The protocol, that we call selective population trapping (SPT) protocol, simply consists in the periodic alternation of RSB laser pulses with measurement and preparation steps. In particular, we consider three steps

(i) A RSB pulse is applied for a time $\tau = 2\pi/(\eta\Omega\sqrt{n_0})$, where $n_0 > 0$ is an integer of our choice that determines the form of the trapped state.

(ii) An unread measurement of the electronic state of the ion is performed at time τ.

(iii) The ion is projected back into its electronic ground state $|g\rangle$.

The effect of this process is illustrated in fig. 1(a). Population of most Fock states cascades down analogously to a sideband-cooling scheme. Nevertheless, the length of the sideband pulse τ matches the red-sideband period of motional Fock states $|n_0 m^2\rangle$, where m is any natural number. All states for which the sideband pulse represents a full Rabi oscillation will remain trapped. Eventually, motional Fock mixtures are generated that have the form

$$\mu_{tr} = \sum_{m=0}^{\infty} p_{tr}(m) \left|n_0 m^2\right\rangle \left\langle n_0 m^2\right|, \tag{3}$$

where the initial population of all states below trap $|n_0(m+1)^2\rangle$ has been deposited in trap $|n_0 m^2\rangle$, so that, for an initial motional state μ_0, we have

$$p_{tr}(m) = \sum_{k=n_0 m^2}^{n_0(m+1)^2-1} \langle k| \mu_0 |k\rangle. \tag{4}$$

For the particular case of an initially thermal distribution μ_0^{th} of inverse temperature β, we have $\langle k| \mu_0^{th} |k\rangle = (1 - e^{-\beta\nu})e^{-\beta\nu k}$, and the final trapped state distribution becomes $p_{tr}^{th}(m) = e^{-\beta\nu n_0 m^2} - e^{-\beta\nu n_0 (m+1)^2}$. Some examples are presented in fig. 1(b).

The state described by eq. (3) is a non-thermal probability distribution. The function $p_{tr}(m)$ may even be non-monotonous: the position of its maximum depends only on the initial state μ_0 and the time τ, as it can be clearly seen in fig. 1(b). Since the protocol concentrates population in a few trapping levels, it is expected to reduce the entropy of the state, as shown in fig. 1(c). A proof that this is always the case for an initially diagonal state in the Fock basis can be found in the Appendix.

Periodic electronic state measurement and preparation (steps 2 and 3 of the protocol) may be implemented by using electronic shelving techniques [24]: an additional laser resonantly couples $|e\rangle$ to a higher excited level of the ion $|f\rangle$, which has a fast decay rate back to the electronic ground state of the system, see fig. 1(d). This technique is also commonplace in implementations of standard sideband cooling in order to increase cooling rates.

3. Kraus Maps Analysis and Steady State

As a way to analyze the dynamics of the motional degrees of freedom, we employ the Kraus sum representation of quantum processes [25]. The effect of the sideband, measurement and preparation pulses are summarized by Kraus maps K_e or K_g, depending on the outcome of the electronic state measurement. Disregarding the measurement outcome, the unconditional evolution of the density matrix $\mu(\tau)$ of the motional degrees of freedom is

$$\mu(\tau) = \sum_{i=e,g} K_i \mu_0 K_i^{\dagger}. \tag{5}$$

Kraus maps satisfy the condition $\sum_{i=e,g} K_i^\dagger K_i = \mathbf{1}$. Under the described protocol, they are computed as $K_i = \langle i | U(\tau) | g \rangle$, with $U(\tau) = e^{-iH_{RSB} \cdot \tau}$ being the unitary evolution operator associated with the red sideband pulse. The final expressions read

$$K_g = \sum_{n=0}^{\infty} \cos\left(\sqrt{n} \frac{\eta \Omega}{2} \tau\right) |n\rangle \langle n|, \tag{6}$$

$$K_e = -\sum_{n=0}^{\infty} \sin\left(\sqrt{n+1} \frac{\eta \Omega}{2} \tau\right) |n\rangle \langle n+1|. \tag{7}$$

Since by step 3 of the protocol the electronic state is prepared back into $|g\rangle$, the same set of Kraus maps can be used to describe repeated iterations of the SPT-Protocol. This is a useful property in order to extract the steady state of the Fock state populations.

From the structure of the Kraus maps it can be seen that the evolution of populations and coherences is decoupled. In particular, we may describe the stroboscopic evolution of the vector of populations $\mathbf{p}(t) = (p_0, p_1, ..., p_n, p_{n+1}, ...)^T$ [with $p_n = \langle n | \mu(t) | n \rangle$ and $t = k\tau$ any integer multiple of τ] by means of the dynamical map $\mathcal{E}(\tau)$. It is a matrix whose components are related to the Kraus maps

$$\mathcal{E}_{mn}(\tau) = \sum_{i=e,g} \langle m | K_i(\tau) | n \rangle \langle n | K_i^\dagger(\tau) | m \rangle. \tag{8}$$

The steady state populations $\mathbf{p}^{ss}$ satisfy the equation $\mathbf{p}^{ss} = \mathcal{E}(\tau)\mathbf{p}^{ss}$, which implies

$$\sin^2\left(\sqrt{n} \frac{\eta \Omega}{2} \tau\right) p_n^{ss} = \sin^2\left(\sqrt{n+1} \frac{\eta \Omega}{2} \tau\right) p_{n+1}^{ss}. \tag{9}$$

Beyond the trivial solution (which corresponds to $p_0^{ss} = 1$ and $p_n^{ss} = 0$ for any $n > 0$), this equation illustrates the reason for the choice $\tau = 2\pi/(\eta \Omega \sqrt{n_0})$, since it is only for this case that additional solutions exist, corresponding to the trapped states.

4. Displacement Sensitivity and Quantum Metrology

We now analyze the metrological advantage trapped states can have with respect to the ground state in the field of displacement sensitivity. In the spirit of [16], a phase-space displacement α is implemented by letting the ion interact with an external electric field. This corresponds to the state transformation $\mu_{tr} \rightarrow D(\alpha)\mu_{tr} D^\dagger(\alpha)$ with $D(\alpha) = \exp(\alpha a^\dagger - \alpha^* a)$. In the simplest approach, the interaction is interrupted by a state read-out measurement for the motional state $|n\rangle$ of the ion. This measurement carries some information about α. In particular, with the help of the overlap function $\xi(\alpha) = \text{tr}\left\{ |n\rangle \langle n | D(\alpha)\mu_{tr} D^\dagger(\alpha) \right\}$ between the initial and the displaced state one can express the Fisher information of the measurement with

$$\mathcal{F}(\alpha) = \frac{1}{\xi(\alpha)[1 - \xi(\alpha)]} \left[\frac{d\xi(\alpha)}{d\alpha} \right]^2, \tag{10}$$

which can then be used to quantify the metrological gain in comparison to the SQL as

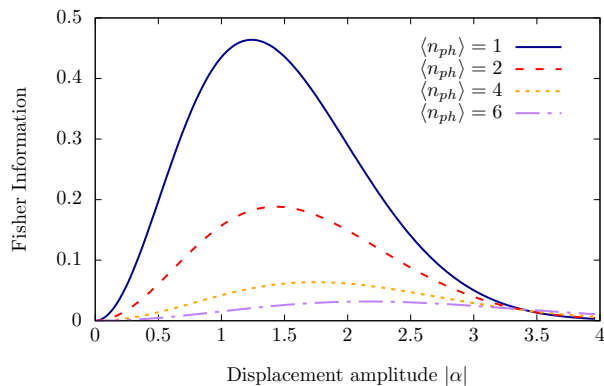$$g = \frac{\mathcal{F}_Q(\alpha)}{\mathcal{F}_{SQL}}, \tag{11}$$

Figure 2. Fisher information of the displacement amplitude $|\alpha|$ carried by a projective measurement of the motional ground state $|0\rangle$ given an initial thermal state of different values of $\langle n_{ph} \rangle$.

where $\mathcal{F}_Q(\alpha) = \max_\alpha \mathcal{F}(\alpha)$ stands for the quantum Fisher information and $\mathcal{F}_{SQL}$ is the Fisher information produced by the motional ground state $|0\rangle$. The quantum Fisher information is then directly linked to the achievable measurement sensitivity $\Delta\alpha$ by means of the Cramer-Rao bound $\Delta\alpha^{CR}$, given by

$$\Delta\alpha \geq \Delta\alpha^{CR} = \frac{1}{\sqrt{N\mathcal{F}_Q(\alpha)}}. \tag{12}$$

More details on the calculations of state overlap and the associated Fisher information are included in the Appendix.

Thermal State   The Fisher information of a thermal state characterized by an average population $\langle n_{ph} \rangle$ is significantly lower than the standard quantum limit and is therefore not appropriate for metrological purposes. As illustrated in fig. 2, the maximum Fisher information decreases with an increasing $\langle n_{ph} \rangle$ and appears at larger values of the displacement amplitude $|\alpha|$. This justifies the use of sideband cooling to achieve higher sensitivities, although trapped states can overcome the SQL without it, as we will now show.

Trapped State   Figure 3 shows the Fisher information of a trapped state as a function of the displacement amplitude $|\alpha|$. We consider trapped states created from thermal states with different values of temperature represented by their initial average phonon number $\langle n_{ph} \rangle$. For each value, two curves are presented, each one corresponding to a measurement for a different Fock state. The blue curve indicates a measurement of the most likely Fock state of the given trapped mixture μ_{tr}, i.e. the Fock state $|n_0 m^2\rangle$ with highest $p_{tr}(m)$. The red curve corresponds instead to a measurement of the next Fock state $|n_0 m^2 + 1\rangle$, which is not a member of the trapping series. Red curves do not feature higher peaks in the Fisher information, they do however result in higher Fisher information values for very small displacement amplitudes. By comparison with fig. 2, it becomes apparent that trapped states produce significantly higher Fisher information
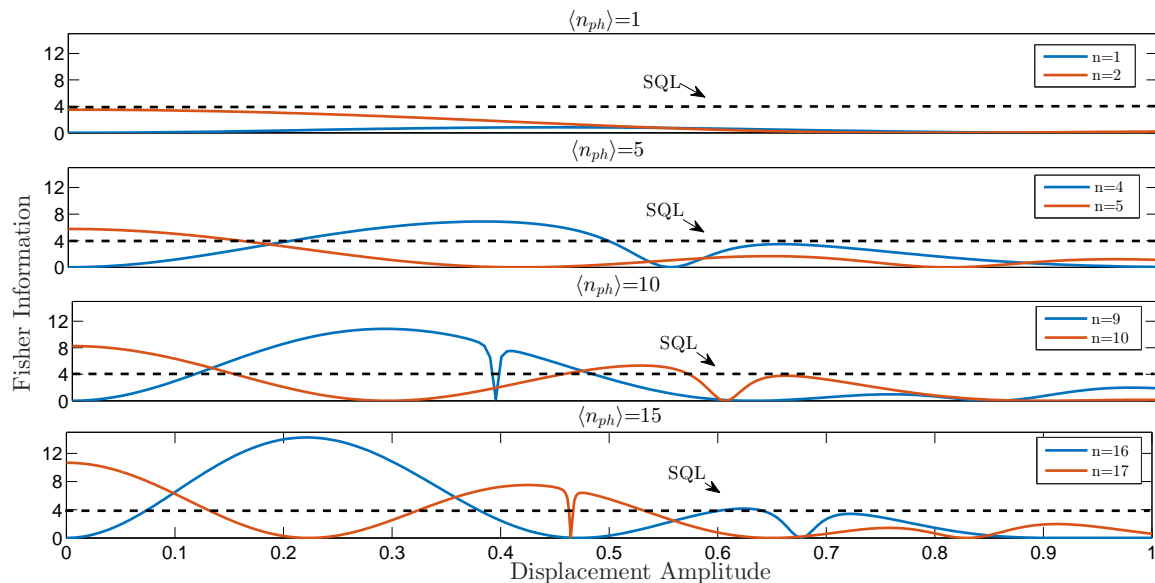
Figure 3. Trapped state Fisher information as a function of the displacement amplitude $|\alpha|$ for different values of the average phonon number of the initial thermal state $\langle n_{ph} \rangle$ and measured Fock state n.

than thermal states. Additionally, the Fisher information exceeds the SQL under certain conditions, as it can be seen in fig. 3 for $\langle n_{ph} \rangle = 5$, $\langle n_{ph} \rangle = 10$ and $\langle n_{ph} \rangle = 15$. As opposed to thermal states, achievable values of Fisher information by trapped states increase with larger initial temperatures. This proves that trapped states can be useful for metrological purposes, since they can provide higher displacement sensitivities than the motional ground state.

In particular, we can expect the following metrological gains:

$$\langle n_{ph} \rangle = 5: \quad g_{SQL} = \frac{\mathcal{F}_{tr}\left(\alpha \approx 0.4\right)}{\mathcal{F}_{SQL}} \approx 1.75 \text{ dB},$$

$$\langle n_{ph} \rangle = 10: \quad g_{SQL} = \frac{\mathcal{F}_{tr}\left(\alpha \approx 0.3\right)}{\mathcal{F}_{SQL}} \approx 2.75 \text{ dB}, \text{ and}$$

$$\langle n_{ph} \rangle = 15: \quad g_{SQL} = \frac{\mathcal{F}_{tr}\left(\alpha \approx 0.24\right)}{\mathcal{F}_{SQL}} \approx 3.5 \text{ dB}.$$

It is worth stressing that trapped states have finite entropy [see fig. 1(c)] and still are expected to provide a metrological gain with respect to the pure ground state (of zero entropy).

5. Blue-Sideband Trapping

Here we extend the idea of selective population trapping for the case of a blue-sideband (BSB) excitation. The SPT protocol stays as defined in sec. 2, with the only exception being that now a BSB transition is implemented in the first step. Since all the analytical derivations for this section are formally identical to the ones detailed in the RSB case,

we are going to simply present the results in a compact form and only focus on the differences between the two processes. The Hamiltonian in this case is also known as anti-Jaynes-Cummings Hamiltonian and is given in the RWA by

$$H_{BSB} = -\frac{i\eta\Omega}{2}\left(a^\dagger\sigma^+ - a\sigma^-\right).$$ (13)

The corresponding Kraus maps have the form

$$K_g' = \sum_{n=0}^{\infty} \cos\left(\sqrt{n+1}\frac{\eta\Omega}{2}\tau\right)|n\rangle\langle n|,$$ (14)

$$K_e' = \sum_{n=0}^{\infty} \sin\left(\sqrt{n+1}\frac{\eta\Omega}{2}\tau\right)|n+1\rangle\langle n|.$$ (15)

Solving for the steady state of these Kraus maps, the following equations arise

$$\sin^2\left(\sqrt{n+1}\frac{\eta\Omega}{2}\tau\right)p_n^{ss} = \sin^2\left(\sqrt{n}\frac{\eta\Omega}{2}\tau\right)p_{n-1}^{ss}.$$ (16)

For a BSB-pulse time $\tau = 2\pi/(\eta\Omega\sqrt{n_0})$, the final mixture now has the form

$$\mu_{tr}' = \sum_{m=1}^{\infty} p_{tr}'(m)\left|n_0 m^2 - 1\right\rangle\left\langle n_0 m^2 - 1\right|,$$ (17)

A difference in comparison to the RSB case is that now the first member of the trapping series can be arbitrarily chosen and is not necessarily the motional ground state $|0\rangle$.

A very interesting feature of the trapped state produced by a BSB excitation is that one can reduce the entropy of the motional degree of freedom (the proof of this is formally equivalent to the one presented in the appendix) by increasing its energy. Additionally, with the BSB version of the protocol it is possible to create mixtures of definite odd Fock state parity, whereas RSB mixtures can be created with definite even parity.

6. Numerical Simulation

So far, the SPT protocol has been presented analytically, assuming a Jaynes-Cummings Hamiltonian [eq. (2)] or an anti-Jaynes-Cummings Hamiltonian [eq. (13)]. Additionally, both the measurement and the spontaneous decay of the ion back to the electronic ground state have been assumed to be instantaneous. In this section, we test the predictions in a more realistic scenario by performing numerical simulations that include both finite ground state preparation time and the full Hamiltonian [eq. (1)].

Lindblad Master Equation and Evolution in Two Steps

In this numerical simulation we model the SPT-Protocol as a two-step process: (1) the unitary evolution of the closed electronic-motional system for time τ and (2) the unread measurement followed by the spontaneous decay of the ion due to photon emission taking an extra time $\tau_{e\to g}$. This is done by means of a master equation in Lindblad

form [26] as given in [27]. It acts on the *total* density matrix ρ, involving both electronic and motional degrees of freedom, and is expressed by the following equation

$$\frac{d}{dt}\rho = -i\left[H, \rho\right] + \frac{\Gamma}{2}\left(2\sigma^{-}\rho\sigma^{+} - \sigma^{+}\sigma^{-}\rho - \rho\sigma^{+}\sigma^{-}\right)$$
$$\equiv \mathcal{L}(\Omega, \Gamma)\rho, \tag{18}$$

where Γ is the decay rate between the two qubit states and $\mathcal{L}$ stands for the Liouvillian of the system. By using the full Hamiltonian from eq. (1), we include the effects of off-resonant carrier and blue sideband excitations, as well as all higher-order Lamb-Dicke terms.

The dynamical map describing the evolution of ρ is the result of the product $\mathcal{E}_{sim}\left(\tau + \tau_{e\rightarrow g}\right) = \mathcal{E}_{d}\left(\tau_{e\rightarrow g}\right) \cdot \mathcal{E}_{u}\left(\tau\right)$, where $\mathcal{E}_{u}\left(t\right) = \exp[\mathcal{L}(\Omega, 0)t]$ represents the unitary part of the evolution (with $\Gamma = 0$) and $\mathcal{E}_{d}(t) = \exp[\mathcal{L}(0, \Gamma)t]$ the dissipative part of the evolution (with $\Omega = 0$). This is illustrated in fig. 4.
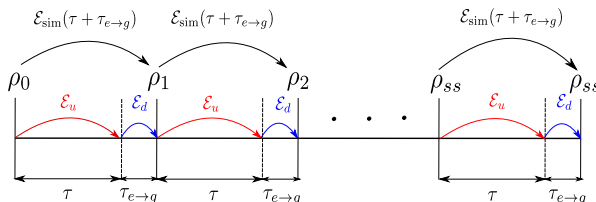

Figure 4. Schematics for the two-step process describing one cycle of the numerical simulation of the SPT-Protocol. The dashed vertical lines represent the end of the unitary interaction and the solid lines the density matrix after a whole cycle of the protocol.

Results and Discussion

We compare the analytical prediction for the population vector $\mathbf{p}_R$ after R repetitions of the SPT protocol as provided by the ideal dynamical map $\mathcal{E}(\tau)$ from eq. (8), $\mathbf{p}_R = \mathcal{E}^R(\tau)\mathbf{p}_0$, and as computed from the numerical simulation, $\rho\left(R\tau + R\tau_{e\rightarrow g}\right) = \mathcal{E}_{sim}^R(\tau + \tau_{e\rightarrow g})\rho\left(0\right)$. This facilitates identification and analysis of the three parametric requirements ($R \gg 1$, $\eta \ll 1$ and $\Omega \ll \nu$) necessary for SPT to work. For simplicity, throughout this section we use $n_0 = 1$. Simulations were performed with a cutoff $\dim_m = 14$ for the motional Hilbert space (maximum Fock state number), which was found to produce sufficient convergence.

Number of Repetitions First, varying the number of repetitions R and comparing the results leads to an understanding of how many applications of the SPT-Protocol are necessary in order to observe the effect of population trapping expected in the steady state. For the parametric regime in which trapped states are well approximated ($\eta \ll 1$ and $\Omega \ll \nu$), we find that $R = 30$ is sufficient to reach a reasonable approximation to the steady state, since higher values do not appreciably modify the distribution.
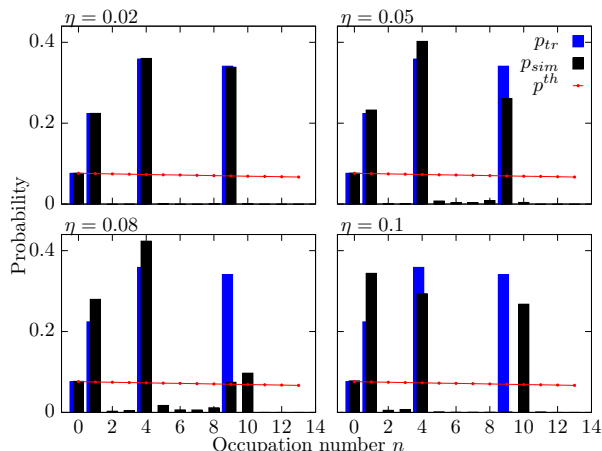
Figure 5. Comparison between the analytical predictions p_{tr} (blue) and simulated results p_{sim} (black) for the probability distribution of Fock populations for $R = 30$ repetitions of the protocol applied on an initially thermal state p^{th} (red) for various values of the Lamb-Dicke parameter. The following parameter values have been used: $n_0 = 1$, $\Omega = 10^{-4}\nu$, $\beta = 0.01\nu^{-1}$, $\delta = \nu$ and $\Gamma_{e\to g} = 1000\nu$.

Lamb-Dicke Parameter   A small η leads to population distributions significantly closer to the analytical predictions, as can be seen in fig. 5. This is due to the Lamb-Dicke approximation $\eta\sqrt{\langle n_{ph}\rangle} \ll 1$, which loses its validity both as n or η increase. For values of $\eta \leq 0.02$, the simulated results completely match the analytical ones after about 20 repetitions of the protocol. Values in the range $0.02 < \eta < 0.06$ only approach the predictions within a margin of about 10%, while for higher values the two predictions are completely incompatible. For larger η, the Lamb-Dicke approximation is no longer valid and one needs to account for higher order terms of the form $a^{\dagger(m+n)}a^m$, which couple states with quantum numbers that vary by n, i.e. $|g, m\rangle \to |e, m + n\rangle$. The role of n in the loss of validity of the Lamb-Dicke approximation is also clear from the simulation: as η increases, lower values of n are affected. As shown in the top right subplot of fig. 5, a small increase in η primarily affects trapping state $n = 9$, while further increase of η (bottom right) unstabilizes the $n = 4$ trapping state as well. Meanwhile the $n = 1$ trapping state remains stable and accumulates the escaped population.

An interesting effect that can be observed in the bottom right subplot of fig. 5, is the formation of a trap at $n = 10$ for $\eta = 0.1$, which cannot be explained within the Jaynes-Cummings type model employed in the previous sections. The trapping at that state is very persistent, and is present even after 1000 repetitions of the protocol. We suspect this behaviour to be due to the Debye-Waller reduction factor of the Lamb-Dicke parameter due to high-order effects [31] and will be investigated elsewhere. At any rate, it is an indication that the concept of selective population trapping could be extended to models that account for all Lamb-Dicke orders.

Rabi Frequency   We now focus on how different Rabi frequencies influence the results, as shown in fig. 6. Increased Ω leads to some population escaping the traps due to
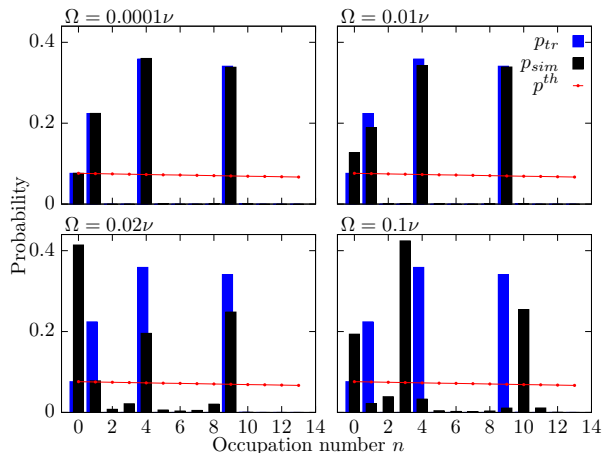
Figure 6. Comparison between the analytical predictions p_{tr} (blue) and simulated results p_{sim} (black) for the probability distribution of Fock populations for $R = 30$ repetitions of the protocol applied on an initially thermal state p^{th} (red) for various values of the Rabi frequency. For all the subplots, the following parameter values have been used: $n_0 = 1$, $\eta = 0.02$, $\beta = 0.01\nu^{-1}$, $\delta = \nu$ and $\Gamma_{e \to g} = 1000\nu$.

off-resonant carrier excitation, as the corresponding term in the Hamiltonian of eq. (1) becomes more important. In order to remain within the regime of validity of the RWA underlying H_{RSB}, we observe that Rabi and trap frequencies require a separation of approximately three orders of magnitude. Values of Ω that are only two orders of magnitude larger than ν quickly destabilize the traps. In contrast to an increased Lamb-Dicke parameter, this affects the lower lying traps first. It has also been observed that, for higher Rabi frequency values that are within the range of about $(0.5 - 1)\%$ of the trap frequency, the analytical result is better reproduced for about twenty repetitions of the protocol, instead of the thirty shown in the figures.

In conclusion, population trapping as described in sec. 2 is experimentally applicable in the regimes given by $\eta \leq 0.02$ and $\Omega \leq 0.005\nu$, which directly results from the approximations made in the derivation of the Hamiltonian in eq. (2).

Conclusions

We have presented a protocol for the creation of a special class of motional states in trapped ions. The protocol is simple and involves the alternate concatenation of red or blue sideband pulses with measurement and preparation pulses. The form of the generated state depends on the duration of the sideband pulses and populates only Fock states proportional to perfect square numbers. The presence in the mixture of excited Fock states makes them especially suitable for motional metrology, improving on the standard quantum limit without the need for long sideband cooling pulses. The protocol works best with small values of the Lamb-Dicke parameter in order to avoid deleterious high-order effects, and small Rabi frequencies to suppress carrier effects. Such a protocol might be applied in a Penning trap to measure the motional frequencies

of a single ion and even extend it to the case of an unbalanced two-ion crystal where the motional modes of the crystal has to be probed [32, 33].

Acknowledgments

References

[1] J. I. Cirac and P. Zoller, "Quantum Computations with Cold Trapped Ions", Phys. Rev. Lett. **74**, 4091 (1995).

[2] D. J. Wineland, "Nobel Lecture: Superposition, entanglement, and raising Schrödinger's cat", Rev. Mod. Phys. **85**, 1103 (2012).

[3] N. Friis, O. Marty, C. Maier, C. Hempel, M. Holzäpfel, P. Jurcevic, M. B. Plenio, M. Huber, C. Roos, R. Blatt, and B. Lanyon, "Observation of Entangled States of a Fully Controlled 20-Qubit System", Phys. Rev. X **8**, 021012 (2018).

[4] P. O. Schmidt, T. Rosenband, C. Langer, W. M. Itano, J. C. Bergquist, and D. J. Wineland, "Spectroscopy Using Quantum Logic", Science **309**, 749 (2005).

[5] D. J. Wineland and D. Leibfried, "Quantum information processing and metrology with trapped ions", Laser Phys. Lett. **8**, 175 (2011).

[6] Andrew D. Ludlow, Martin M. Boyd, Jun Ye, E. Peik, and P. O. Schmidt, "Optical atomic clocks", Rev. Mod. Phys. **87**, 637 (2015).

[7] M. Biercuk, H. Uys, J. Britton, A. P. VanDevender, and J. J. Bollinger, "Ultrasensitive detection of force and displacement using trapped ions", Nature Nanotech. **5**, 646 (2010).

[8] P. Ivanov, N. Vitanov, and K. Singer, "High-precision force sensing using a single trapped ion", Sci. Rep. **6**, 28078 (2016).

[9] R. Shaniv, and R. Ozeri, "Quantum lock-in force sensing using optical clock Doppler velocimetry", Nat. Commun. **8**, 14157 (2017).

[10] The LIGO Scientific collaboration, "Enhanced sensitivity of the LIGO gravitational wave detector by using squeezed states of light", Nat. Photon. **7**, 613–619 (2013).

[11] D. J. Heinzen and D. J. Wineland, "Quantum-limited cooling and detection of radio-frequency oscillations by laser-cooled ions", Phys. Rev. A **42**, 2977 (1990).

[12] J. I. Cirac, A. S. Parkins, R. Blatt, and P. Zoller, " "Dark" squeezed states of the motion of a trapped ion", Phys. Rev. Lett. **70**, 556 (1993).

[13] D. M. Meekhof, C. Monroe, B. E. King, W. M. Itano, and D. J. Wineland, "Generation of Nonclassical Motional States of a Trapped Atom", Phys. Rev. Lett. **76**, 1796 (1996).

[14] D. Kienzler, C. Flühmann, V. Negnevitsky, H.-Y. Lo, M. Marinelli, D. Nadlinger, and J. P. Home, "Observation of Quantum Interference between Separated Mechanical Oscillator Wave Packets", Phys. Rev. Lett. **116**, 140402 (2016).

[15] S. C. Burd, R. Srinivas, J. J. Bollinger, A. C. Wilson, D. J. Wineland, D. Leibfried, D. H. Slichter, and D. T. C. Allcock, "Quantum amplification of mechanical oscillator motion", Science **21**, 1163 (2019)

[16] F. Wolf, C. Shi, J. C. Heip, M. Gessner, L. Pezze, A. Smerzi, M. Schulte, K. Hammerer, and P. O. Schmidt, "Motional Fock states for quantum-enhanced amplitude and phase measurements with trapped ions", Nature Comm. **10**, 1 (2019).

[17] D. Wineland and H. Dehmelt, "Proposed $10^{14}\delta\nu/\nu$ laser fluorescence spectroscopy on Tl$^+$ mono-ion oscillator III (sideband cooling)," Bull. Am. Phys. Soc. **20**, 637 (1975).

[18] G. Morigi, J. Eschner, and C. H. Keitel, "Ground state laser cooling using electromagnetically induced transparency" Phys. Rev. Lett. **85**, 4458 (2000).

[19] N. Scharnhorst, J. Cerrillo, J. Kramer, I. D. Leroux, J. B. Wuebbena, A. Retzker, and P. O. Schmidt, "Experimental and theoretical investigation of a multimode cooling scheme using multiple electromagnetically-induced-transparency resonances", Phys. Rev. A **98**, 023424 (2018).

[20] J. Cerrillo, A. Retzker, and M. B. Plenio, "Double-path dark-state laser cooling in a three-level system" Phys. Rev. A **98**, 013423 (2018).

[21] J. Cerrillo, A. Retzker, and M. B. Plenio, "Fast and Robust Laser Cooling of Trapped Systems", Phys. Rev. Lett. **104**, 043003 (2010).

[22] W. Neuhauser, M. Hobenstatt, P. Toschek, and H. Dehmelt, "Optical-Sideband Cooling of Visible Atom Cloud Confined in Parabolic Well", Phys. Rev. Lett. **41**, 233 (1978) .

[23] E. T. Jaynes and F. W. Cummings, "Comparison of quantum and semiclassical radiation theories with application to the beam maser", Proc. IEEE **51**, 89 (1963).

[24] D. Stevens, J. Brochard, and A. M. Steane, "Simple experimental methods for trapped-ion quantum processors", Phys. Rev. A **58**, 2750 (1998).

[25] K. Kraus, A. Böhm, J. D. Dollard and W. H. Wootters, "States, Effects, and Operations Fundamental Notions of Quantum Theory. Lectures in Mathematical Physics at the University of Texas at Austin", Lecture Notes in Physics, 190 (Springer Berlin, 1983).

[26] G. Lindblad, "On the generators of quantum dynamical semigroups", Comm. Math. Phys. **48**, 119 (1976).

[27] S. Haroche, Exploring the quantum atoms, cavities and photons, Oxford graduate texts (Oxford University Press, 2006).

[28] J. Neumann, Mathematische Grundlagen der Quantenmechanik , 2nd ed. (Berlin, 1996).

[29] A. Wuensche, Quantum Optics: Journal of the European Optical Society Part B 3, 359 (1991).

[30] H. van Haeringen and L. P. Kok, Mathematics of Computation 41, 778 (1983).

[31] D. J. Wineland, C. Monroe, W. M. Itano, D. Leibfried, B. E. King, and D. M. Meekhof, "Experimental Issues in Coherent Quantum-State Manipulation of Trapped Atomic Ions", J. Res. Natl. Inst. Stand. Technol. **103**, 259 (1998).

[32] M. J. Gutiérrez, J. Berrocal, F. Domínguez, I. Arrazola, M. Block, E. Solano, and D. Rodríguez, "Dynamics of an unbalanced two-ion crystal in a Penning trap for application in optical mass spectrometry", Phys. Rev. A **100**, 063415 (2019).

[33] J. Cerrillo, D. Rodríguez, "Motional quantum metrology in a Penning trap", Eur. Phys. Lett. **134**, 38001 (2021).

Appendix A. Trapped and Thermal State Entropy

The Von Neumann entropy [28] of the system described by a density matrix μ is given by

$$S = -k_B \text{tr} \left(\mu \ln \mu \right), \tag{A.1}$$

which for a diagonal density matrix simplifies to

$$S = -k_B \sum_{m=0}^{\infty} p_m \cdot \ln \left(p_m \right), \tag{A.2}$$

and essentially quantifies the degree of mixedness for a given state. Since in a trapped state there are significantly fewer states populated, one would expect a lower entropy compared to the thermal state that was used to produce it. The following table shows the first few probabilities involved in the sum of eq. (A.2) for both a diagonal and a trapped state, assuming $n_0 = 1$, in order to get an idea on how they relate to each other.

Thermal	p_0	p_1	p_2	p_3	p_4
Trapped	p_0	$\sum_{m=1}^{3} p_m$	0	0	$\sum_{m=4}^{8} p_m$

It is apparent that the contribution to entropy generated by three states with probabilities p_1, p_2 and p_3 respectively is replaced in the trapped state case by the contribution of a single state of total probability $p_1 + p_2 + p_3$.

In general, we have trapped state probabilities

$$p_{tr}(m) = \sum_{k=A}^{B} p_k, \tag{A.3}$$

where $A \equiv n_0 \cdot m^2$ and $B \equiv n_0 \left(m + 1\right)^2 - 1$. The contribution to the entropy corresponding to a single trap and the states until the next trap is

$$p_{tr}(m) \ln\left[p_{tr}(m)\right] = \ln\left[p_{tr}(m)\right] \sum_{k=A}^{B} p_k. \tag{A.4}$$

If we compare it to the contribution to the entropy of the same states in the original distribution

$$\sum_{k=A}^{B} p_k \ln\left(p_k\right) = p_A \ln\left(p_A\right) + p_{A+1} \ln\left(p_{A+1}\right) + \dots + p_B \ln\left(p_B\right). \tag{A.5}$$

Considering that $p_{tr}(m) > p_k$ with k between $A \equiv n_0 \cdot m^2$ and $B \equiv n_0 \left(m + 1\right)^2 - 1$ leads to $\ln\left[p_{tr}(m)\right] > \ln\left(p_k\right)$. In combination with equations (A.4) and (A.5) we get

$$p_{tr}(m) \ln\left[p_{tr}(m)\right] > \sum_{k=A}^{B} p_k \ln\left(p_k\right). \tag{A.6}$$

Summing over the remaining traps and multiplying with $-k_B$ yields the trapped entropy S_{tr} and original entropy S_0 the predicted result

$$S_{tr} < S_0. \tag{A.7}$$

Appendix B. State Overlap

For a prepared state of the form $\mu_0 = \sum_{m=0}^{\infty} p_m \left|m\right\rangle \left\langle m\right|$ the state overlap between the pure state and displaced prepared state can be calculated by

$$\xi\left(\alpha\right) = \mathrm{tr} \left\{ \left|n\right\rangle \left\langle n\right| D\left(\alpha\right) \sum_{m=0}^{\infty} p_m \left|m\right\rangle \left\langle m\right| D^{\dagger}\left(\alpha\right) \right\}$$

$$= \sum_{m=0}^{\infty} p_m \left|\left\langle n\right| D\left(\alpha\right) \left|m\right\rangle\right|^2.$$

The general formula for the scalar product between two displaced Fock states as given in [29] is

$$\left\langle n\right| D^{\dagger}\left(\beta\right) D\left(\alpha\right) \left|m\right\rangle = \sqrt{\frac{m!}{n!}} \left(\alpha - \beta\right)^{n-m} \left\langle \beta\right| \alpha\rangle \, \mathcal{L}_m^{n-m} \left\{\left(\alpha - \beta\right)\left(\alpha^* - \beta^*\right)\right\} \tag{B.1}$$

with $\left\langle \beta\right| \alpha\rangle = \exp\left\{\alpha\beta^* - \frac{1}{2}\left(\alpha\alpha^* + \beta\beta^*\right)\right\}$.

Inserting $\beta = 0$ gives

$$\xi\left(\alpha\right) = e^{-|\alpha|^2} \sum_{m=0}^{\infty} p_m \frac{m!}{n!} |\alpha|^{2(n-m)} \left\{ \mathcal{L}_m^{n-m}\left(|\alpha|^2\right) \right\}^2, \tag{B.2}$$

with $\mathcal{L}_\mu^\nu\left(x\right)$ being the generalized Laguerre polynomials as defined in [30].

Inserting the thermal and trapped probability distribution in eq. (B.2) gives the respective overlap expressions.

Appendix C. Fisher Information

The Fisher information is a measure of how quickly a probability distribution $P\left(x|\theta\right)$ changes with respect to the parameter θ. In order to derive an analytical expression for the Fisher information we follow the method from [16].

The precision of an estimation is limited by the Cramer-Rao bound as

$$\Delta\theta_{est} \geq \Delta\theta_{CR} = \frac{1}{\sqrt{N\mathcal{F}\left(\theta\right)}}, \tag{C.1}$$

where θ_{est} is an arbitrary estimator for θ, N is the number of repeated measurements, and

$$\mathcal{F}\left(\theta\right) = \sum_x \frac{1}{P\left(x|\theta\right)} \left[\frac{\partial P\left(x|\theta\right)}{\partial\theta} \right]^2 \tag{C.2}$$

is the classical Fisher Information. In metrological applications, one is interested in maximizing the precision estimation of the parameter θ. For this purpose, a minimum $\Delta\theta_{CR}$, or equivalently a maximum $\mathcal{F}\left(\theta\right)$ is required.

The probability distribution $P\left(x|\theta\right) = \mathrm{tr}\left\{\Pi_x\mu\left(\theta\right)\right\}$ depends on the quantum state $\mu\left(\theta\right)$ and the choice of the performed measurement, described by the projectors $\{\Pi_x\}$. For processes where the parameter θ is imprinted by a unitary process, i.e. $\mu\left(\theta\right) = U\left(\theta\right)\mu_0 U^\dagger\left(\theta\right)$, the Fisher information has a lower bound given by

$$\mathcal{F}\left(\theta\right) \geq \frac{1}{\left(\Delta M\right)_{\mu(\theta)}^2} \left[\frac{\partial \langle M \rangle_{\mu(\theta)}}{\partial\theta} \right]^2, \tag{C.3}$$

where $\langle M \rangle_{\mu(\theta)} = \mathrm{tr}\left\{M\mu\left(\theta\right)\right\}$ is the mean value and $\left(\Delta M\right)_{\mu(\theta)}^2 = \langle M^2 \rangle_{\mu(\theta)} - \langle M \rangle_{\mu(\theta)}^2$ the variance of the measured observable $M = \sum_x x\Pi_x$.

If there exist only two possible outcomes from a measurement, $x = 0, 1$, this bound is tight. Considering that the probabilities must add up to one, $P\left(0|\theta\right) = 1 - P\left(1|\theta\right)$ and the variance becomes

$$\left(\Delta M\right)_{\mu(\theta)}^2 = P\left(1|\theta\right)\left[1 - P\left(1|\theta\right)\right]. \tag{C.4}$$

Let us now consider the metrological protocol described in the manuscript. Starting with a state ρ_0, we are interested in how a displacement $D(\alpha)$ affects the probability distribution of the state. In other words, we investigate how sensitive the ion is to that displacement. The higher the sensitivity (quantified by the Fisher information), the

more precise the parameter estimation is for the parameter $\theta = \alpha$. The displacement operator is unitary and transforms the density matrix as

$$\mu\left(\alpha\right) = D\left(\alpha\right)\mu_0 D^\dagger\left(\alpha\right). \tag{C.5}$$

A projective measurement for a pure Fock state $|n\rangle\langle n|$ has only two possible outcomes, and therefore the bound (C.3) is tight and the measured observable M takes the form

$$M = \sum_{x=0,1} x\Pi_x = |n\rangle\langle n|. \tag{C.6}$$

This results in a mean value of

$$\langle M\rangle_{\mu(\alpha)} = \mathrm{tr}\left\{M\mu\left(\alpha\right)\right\} = \xi\left(\alpha\right). \tag{C.7}$$

Combining this with $P\left(1|\alpha\right) = \mathrm{tr}\left\{\Pi_1\mu\left(\alpha\right)\right\} = \xi\left(\alpha\right)$ and the tightness of the bound (C.3) results in

$$\mathcal{F}\left(\alpha\right) = \frac{1}{\xi\left(\alpha\right)\left[1 - \xi\left(\alpha\right)\right]}\left[\frac{d\xi\left(\alpha\right)}{d\alpha}\right]^2. \tag{C.8}$$